Molecular Therapy
Methods & Clinical Development
Original Article

Integrase-Deficient Lentiviral Vector as an All-in-One Platform for Highly Efficient CRISPR/Cas9-Mediated Gene Editing

Pavel I. Ortinski,[1] Bernadette O'Donovan,[1] Xiaoyu Dong,[1,2] and Boris Kantor[1,2,3]

[1]Department of Pharmacology, Physiology, and Neuroscience, University of South Carolina School of Medicine, Columbia, SC 29208, USA; [2]Department of Pharmacology, Physiology, and Neuroscience, Viral Vector Core, University of South Carolina School of Medicine, Columbia, SC 29208, USA

The CRISPR/Cas9 systems have revolutionized the field of genome editing by providing unprecedented control over gene sequences and gene expression in many species, including humans. Lentiviral vectors (LVs) are one of the primary delivery platforms for the CRISPR/Cas9 system due to their ability to accommodate large DNA payloads and sustain robust expression in a wide range of dividing and non-dividing cells. However, long-term expression of LV-delivered Cas9/guide RNA may lead to undesirable off-target effects characterized by non-specific RNA-DNA interactions and off-target DNA cleavages. Integrase-deficient lentiviral vectors (IDLVs) present an attractive means for delivery of CRISPR/Cas9 components because: (1) they are capable of transducing a broad range of cells and tissues, (2) have superior packaging capacity compared to other vectors (e.g., adeno-associated viral vectors), and (3) they are expressed transiently and demonstrate very weak integration capability. In this manuscript, we aimed to establish IDLVs as a means for safe and efficient delivery of CRISPR/Cas9. To this end, we developed an all-in-one vector cassette with increased production efficacy and demonstrated that CRISPR/Cas9 delivered by the improved IDLV vectors can mediate rapid and robust gene editing in human embryonic kidney (HEK293T) cells and post-mitotic brain neurons in vivo, via transient expression and with higher gene-targeting specificity than the corresponding integrase-competent vectors.

INTRODUCTION

CRISPR/Cas systems are used by various bacteria and archaea to defend against viruses and other foreign nucleic acids (reviewed in Horvath and Barrangou[1] and Marraffini and Sontheimer[2]). The adaptation of this system for gene editing in mammals has had a considerable impact on development of disease models, identification and validation of novel therapeutic targets, and correction of genetic mutations.[3–5] Lentiviral vectors (LVs) are an important means of delivering CRISPR/Cas9 components due to their ability to accommodate large DNA payloads and efficiently transduce a wide range of dividing and non-dividing cells. LVs also display low cytotoxicity and immunogenicity and have a minimal impact on the life cycle of the transduced cells (reviewed in Kantor et al.[6]). Such features have led to LVs being used as the gene-editing regimen of choice to treat HIV-1, HBV, and HSV-1 infections, as well as to correct defects underlying human hereditary diseases, such as cystic fibrosis.[7–10] Despite these successes, this system suffers from significant drawbacks. Permanently expressed CRISPR/Cas9 may facilitate undesirable off-target effects, hindering their utility for genome-editing applications that require high levels of precision. Indeed, rise of promiscuous interactions with off-target genes due to excess guide RNA (gRNA)/Cas9 is well-documented.[11,12] Furthermore, sustained expression of gRNA/Cas9 in vitro increases the tolerability of mismatches in the guide-matching region and the protospacer adjacent motif (PAM), thereby promoting non-specific double-strand breaks (DSBs).[13,14] Along the same lines, the ratio of insertions and deletions (indels) at off-target versus target sites in vivo increases with higher Cas9 and gRNA concentrations.[15] These results suggest that transient delivery platforms using a "hit and run" strategy for permanent modification of the targeted loci would be beneficial for high-precision gene editing. Several transient-delivery systems have been developed and employed to minimize non-specific effects of the CRISPR/Cas9 system (reviewed in Nelson and Gersbach[16]). For example, it has been recently shown that direct delivery of purified Cas9 protein and single gRNA (sgRNA) into cells results in reduced off-target effects compared to the delivery of plasmid sequences encoding Cas9 and sgRNA.[12] Furthermore, it was demonstrated that Cas9-sgRNA ribonucleoprotein (RNP)-mediated DNA cleavage is followed by their almost instant degradation and clearance from the cells, which suggests that gene editing might only require a short-term presence of its components.[12] More importantly, the high turnover rate of rapidly degraded RNPs corresponded to a reduced rate of off-target mutations. However, low transduction efficiency remains a serious limitation of RNPs and other non-viral delivery platforms. To overcome this limitation, a lentivirus-prepackaged Cas9 protein (Cas9P LV) system was developed recently and was shown to be effective

Received 9 January 2017; accepted 12 April 2017;
http://dx.doi.org/10.1016/j.omtm.2017.04.002.

[3]Present address: Department of Neurobiology, Duke University Medical Center, Durham, NC 27710, USA

Correspondence: Boris Kantor, Duke Department of Neurobiology-School of Medicine, Bryan Research Building, Rm. 213-311 Research Drive, Durham, NC 27710, USA.
E-mail: boris.kantor@duke.edu

for disruption of gene expression in naive T cells.[17] Significantly, transiently delivered Cas9 showed high target specificity and induced no measurable indels at off-target DNA sites. However, production titers of the prepackaged-Cas9 system were observed to be lower than those of conventional LVs.[17]

Conversely, production titers are traditionally high with adeno-associated vectors (AAVs) that have become a widely adopted platform for delivery of CRISPR/Cas9 components in recent years (reviewed in Nelson and Gersbach[16]). Indeed, Platt and colleagues[18] successfully packaged a *Streptococcus pyogenes* (SpCas9)/sgRNA construct into AAV particles for in vivo modeling of loss-of-function mutations in *P53* and *LKB1* genes in mouse lung adenocarcinomas. However, the large size of the SpCas9 gene (4.2 kb) imposes a significant burden on the packaging capacity of AAVs. To overcome this bottleneck, Oskar Ortiz's group recently developed a split-intein Cas9 system that can be separated into two AAV cassettes.[19] This approach allows for increase in overall packaging capacity, but necessitates production and co-transduction of two AAV vectors. The discovery of a shorter, but equally potent Cas9 enzyme derived from *Staphylococcus aureus* (SaCas9) led to the development of SaCas9/guide RNA system that could be efficiently packaged and delivered by AAV vectors.[20] This system was shown to efficiently target the cholesterol regulatory gene *PCSK9* in the mouse liver.[20] Nevertheless, the packaging efficacy of all-in-one AAV vector systems, especially those intended for clinical applications, needs further improvement to efficiently accommodate multiple components, including the 3.2-kb SaCas9, the RNA polymerase II (Pol II) promoter and poly(A), a nuclear localization signal (NLS), sgRNA(s), and the RNA polymerase III (Pol III) promoter(s), as well as other *cis*-acting elements, such as woodchuck hepatitis post-transcriptional regulatory element (WPRE).[21]

Episomal IDLVs are an ideal platform for delivery of large genetic cargos where only transient expression of the transgene is desired (reviewed in Kantor et al.,[6] and Wanisch and Yáñez-Muñoz[22]).[23–32] We demonstrated more recently that IDLVs retained residual (integrase-independent and illegitimate) integration rates of ~0.2%–0.5% (one integration event per 200–500 transduced cells), which could be further reduced by packaging a novel 3′ polypurine tract (PPT)-deleted lentiviral vector into integrase-deficient particles.[33] Several studies have demonstrated broadly similar levels of illegitimate integration.[27,34,35]

IDLVs have garnered significant interest among researchers for precise in vivo analysis of genetic diseases, since they significantly reduce the risk of insertional mutagenesis inherent in integrating delivery platforms. For example, Thrasher et al.[36] and Suwanmanee et al.[37] have successfully employed IDLVs in mouse models as gene replacement therapies for degenerative retinal disease and hemophilia B, respectively. Furthermore, the efficacy of IDLVs in cancer immunotherapy and as a means of inducing protective immune responses to human pathogens has been characterized in different experimental settings.[38–40] A growing body of literature describes IDLVs carrying zinc-finger nucleases as an effective means of gene editing for clinical and basic science applications[28,30–32]. For instance, Lombardo and colleagues[28] have successfully employed non-integrating vectors as a means of avoiding genotoxicity associated with continuous expression of zinc-finger nucleases (ZFNs) and for delivering the donor DNA template required for DNA repair-mediated gene editing. These researchers demonstrated that the IDLV-ZFNs system is capable of effectively disrupting expression from the gene encoding the HIV-1-co-receptor CCR5. Additionally, Joglekar and colleagues[30] successfully employed IDLVs to deliver ZFNs and donor templates for site-specific gene modification at the human adenosine deaminase (*hADA*) locus in primary T-lymphocytes. Most recently, Hoban and colleagues[41] demonstrated efficient gene editing of the mutated human β-globin gene in CD34+ hematopoietic stem and progenitor cells by co-delivering CRISPR/Cas9 reagents and donor templates via IDLVs.

The ability to simultaneously deliver Cas9 and sgRNA through a single vector enables facile and robust in vivo gene editing, which is particularly advantageous for developing a translatable gene therapy products (reviewed in Maeder and Gersbach[42]). In the current manuscript, we aimed to establish an all-in-one IDLV-CRISPR/Cas9 system for efficient gene editing in vitro and in vivo. To this end, we designed and tested novel non-integrating vectors carrying binding sites for the transcription factor Sp1 in the expression cassette. We demonstrate that these vectors permit efficient, rapid, and sustainable CRISPR/Cas9-mediated gene editing in HEK293T cells and post-mitotic brain neurons in vivo. Furthermore, we demonstrate that the IDLV-CRISPR/Cas9 system is expressed transiently and has a significantly lower capacity to induce off-target mutations than its integrating counterparts have. Taken together, our findings validate IDLVs as a robust, effective, and safe means for in vivo delivery of programmable nucleases, with substantial advantages over other delivery platforms.

RESULTS

Modifications to the Lentiviral Vector System for Delivery of CRISPR/Cas9 Components

We started with the titer-optimized lentiCRISPR-v2[43] in which we removed the unnecessary buffer sequences (~2 kb) and introduced a unique restriction site for reducing unwanted recombination, increasing growth rates, and enabling easy screening for sgRNA-positive clones in bacteria (Figure 1A, upper panel; Materials and Methods). LentiCRISPR-v2 is characterized by higher production yields compared to the original CRISPR-v1vector; nevertheless, its titers are still lower than is typical of conventional LVs. To improve vector titers, we sought to reinstate binding site(s) for the transcription factor Sp1 into the shorter version of lentiCRISPR-v2. The idea is premised on previous data demonstrating that Sp1 plays a pivotal role in the life cycle of wild-type HIV-1, but is deleted from most of the vector cassettes.[44–47] We first cloned two copies of the Sp1 binding site upstream of the U6-promoter (Figure 1A, lower panel). Next, we generated ICLVs (integrase-competent) and IDLVs (integrase-deficient) with or without Sp1 by packaging corresponding vector

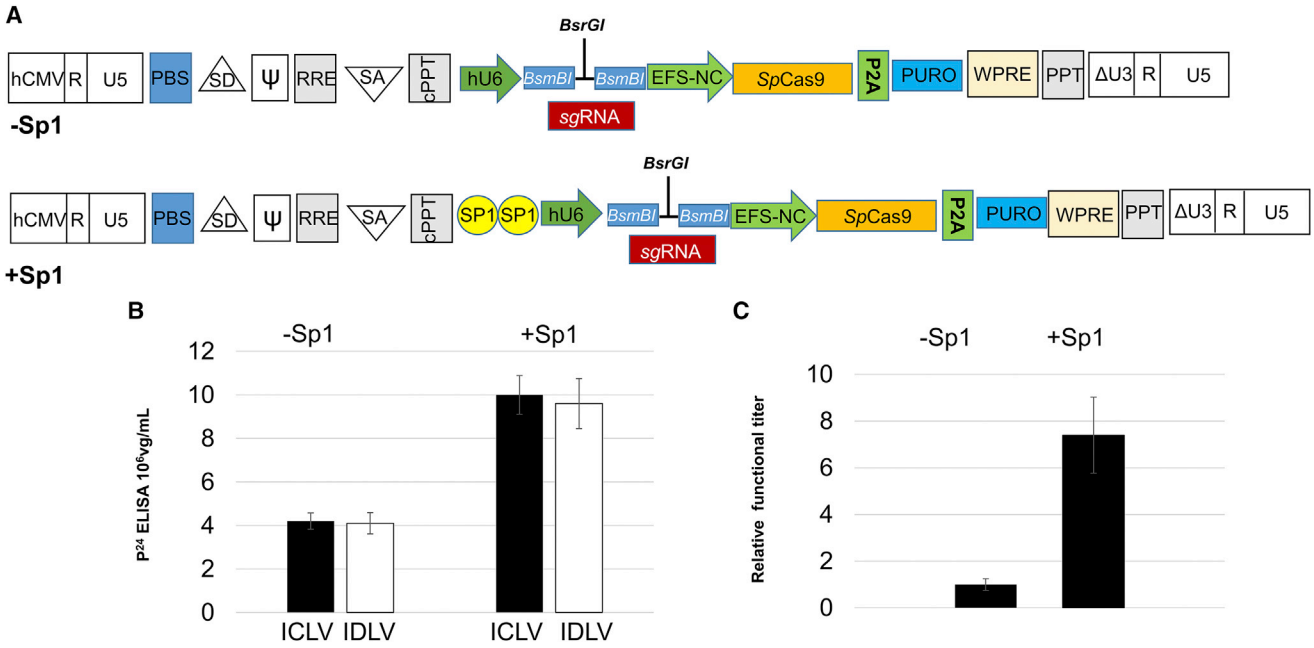

Figure 1. Vector Production

(A) A schematic map of the vector cassette. A shorter version of pLentiCRISPRv2 was created to include a unique BsrGI restriction enzyme site flanked by two BsmBI sites to be used for cloning sgRNAs. Other regulatory elements of the vectors include a primer binding site (PBS), splice donor (SD) and splice acceptor (SA), central polypurine tract (cPPT) and PPT, Rev Response element (RRE), WPRE, and the retroviral vector packaging element, psi (ψ) signal. A human cytomegalovirus (hCMV) promoter, a core-elongation factor 1α promoter (EFS-NC), and a human U6 promoter are highlighted. (B) Production titers of the vectors with and without Sp1 binding sites as determined by p^{24}ELISA assay. The results are recorded in copy numbers per milliliter, equating 1 ng of p^{2}*gag* to 1 × 10^{4} viral particles. (C) The overall ICLV production titer determined by counting puromycin-resistant colonies. The results are shown as the ratio between number of colonies obtained from the vector with and without Sp1. The bar graph data represents mean ± SD from triplicate experiments.

cassettes into either integrase-wild-type, or integrase-deficient (D64E mutant) viral particles supplemented with vesicular stomatitis virus G envelope (VSV-G). The production titers of the resulting vectors were measured using a p24*gag* ELISA assay. As shown in Figure 1B, IDLVs harboring Sp1 binding sites demonstrated a ~2.5-fold increase in p24 production compared to the parental vector. Interestingly, we observed a similar level of increase in p24 production with ICLVs (Figure 1B). We further assessed the production efficiency of ICLVs with or without Sp1 using an antibiotic-resistance (puromycin) colony forming assay. We observed a ~7-fold increase in the number of puromycin-resistant colonies with ICLVs harboring Sp1 binding sites compared to the no-Sp1 vector counterpart (Figure 1C).

Knockout Efficiency of IDLV-Based CRISPR/Cas9

To examine knockout efficiency of the new vector system, we designed three sgRNA constructs targeting different regions of enhanced green fluorescent protein (eGFP) stably expressed in HEK293T cells. We first packaged a sgRNA-to-GFP/Cas9 expression cassette into integrase-wild-type particles and assessed target gene knockout in the reporter GFP-positive HEK293T cells using flow cytometry. The sgRNA1/Cas9 vector that demonstrated near complete depletion of the GFP signal was selected for further evaluation (Figure S1). Next, we asked if sgRNA1/Cas9 packaged into integrase-deficient particles could induce efficient GFP knockout in dividing cells. To this end, IDLV-sgRNA1/Cas9 and ICLV-sgRNA/Cas9 vectors were transduced into 293T cells and knockout levels were evaluated at 7, 14, and 21 days post-transduction (pt) by flow cytometry. Both integrated and episomal vectors displayed a ~5-fold reduction in the number of GFP-positive cells as early as 7 days pt, with a nearly complete signal depletion observed by 21 days pt (Figure 2). These results clearly demonstrate that CRISPR/Cas9 delivered by IDLVs is capable of mediating rapid, robust, and sustained gene editing in dividing cells. Next, we assessed the integration capacity of non-integrating vectors to rule out the possibility that overexpressed CRISPR/Cas9 may alter the rate of integration. We transduced 293T cells with integrating and non-integrating vectors carrying sgRNA1/Cas9 as described above, cultured the cells for 3 weeks to dilute out non-integrated genomes, and finally, isolated viral DNA from these cells for subsequent analysis with real-time PCR. The rate of integrase-independent (illegitimate) integration of IDLVs determined as a ratio between copy numbers at week 3 and at 24 hr post transduction was found to be ~0.8% (Figure S2). This finding suggests that CRISPR/Cas9 does not significantly alter the integration capacity of non-integrating vectors since only slightly lower rates (0.2%–0.5%) of integration were reported previously for non-CRISPR-vectors.[33] The integration frequency of ICLV-CRISPR/Cas9 was found to be ~30%, also consistent with our previous observations (Figure S2).[33]

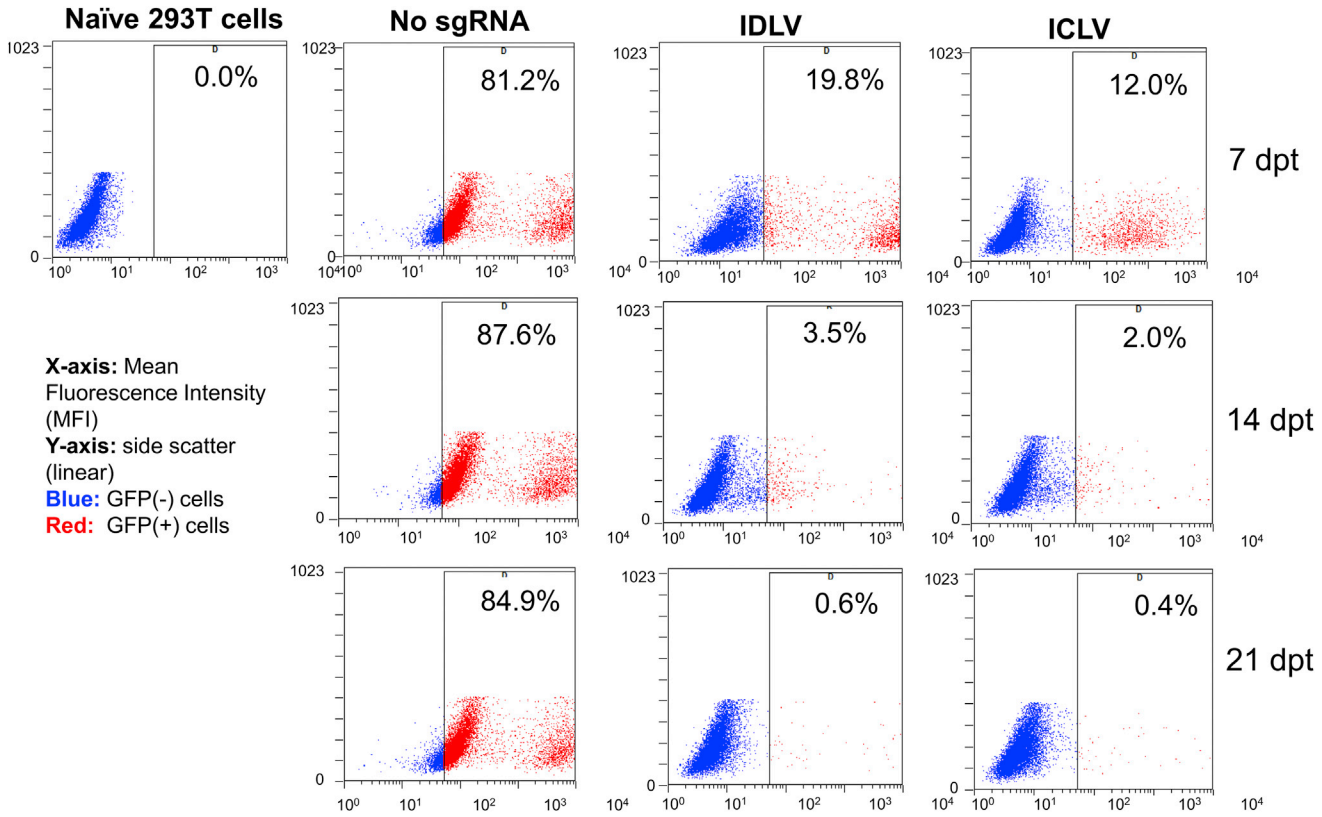

Figure 2. CRISPR/Cas9-Mediated Knockout

eGFP-sgRNA1/Cas9 packaged into IDLV and ICLV particles was transduced into HEK293T-eGFP cells. The knockout levels were evaluated using FACS at days 7, 14, and 21 pt (Materials and Methods). A percentage of GFP-positive cells remaining after transduction was recorded. Naive (not transduced with GFP virus) cells were used as the negative control. The HEK293-eGFP cells transduced with vector carrying no-sgRNA (no-sgRNA) were used as the control. The y axis represents side scatter. The x axis represents MFI.

On-Target Mutations following Transduction with IDLV and ICLV

Having established the ability of the IDLV-CRISPR/Cas9 system to mediate robust and sustained gene editing in dividing cells, we next examined target-specificity of the vectors. We employed T7 endonuclease I to detect mis-annealed DNA that form upon CRISPR/Cas9-induced DSBs. Using the reporter system described in Figure 2, we observed efficient DNA cleavage within the target gene *GFP* at 7 days pt (Figure 3A). Mutations were not observed in naive (untransduced) cells or upon incubation with non-sgRNA-vector (Figure 3A, 1 and 6, respectively). Additionally, we extracted gDNA from ICLV and IDLV-transduced cells (Figure 3B), amplified them with the primers that flank the target GFP sequence, cloned the PCR products into the pCR2.1 TOPO vector (Thermo Fisher), and sequenced them. Analysis of the sequencing data revealed that indels were present in the target sequences at rates 84% and 80% for the ICLV and IDLV vectors, respectively (Figure 3B). Consistent with earlier observations, we saw a random pattern of mutations formed at the target site.[15]

To comprehensively evaluate the off-target capacity of IDLVs, we adopted a whole-exome sequencing (WES) analysis (see description in Materials and Methods). We applied the following criteria to separate potential Cas9-induced DSBs from background DSBs. First, sequences with less than 30 total reads (×30) were not counted. Second, all known variants derived from dbSNPs were omitted. Third, we required indels to be in the frequency range of 1 to 25; higher rates were excluded as potential SNPs and lower rates were considered background noise. Fourth, we excluded sites showing "clustered hot-spots" in which high variability in mutations rates is found within neighboring sequences that represent indels that are likely to arise by technical artifacts and repetitive sequences errors.[48,49] Fifth, indels with no PAM, or with PAM located >10 bp away from seed sequence, or if guide-seed mismatch was more than 5 bps were filtered out as likely technical artifacts[5,15,20,50] (the "seed sequence" has been defined as 10-most proximal nucleotides to PAM).[3,51] Using these criteria, we identified 16 genes in which ICLV-CRISPR/Cas9 induced noticeable changes (Figure 3C). The frequencies of ICLV-induced indels at these sequences were in the range of 3.4%–24% (Figure 3C). In contrast, IDLV-CRISPR/Cas9 demonstrated significantly weaker capability to induce off-target indels at these sequences (Figure 3C). With IDLVs, we observed close-to-baseline indels frequency in seven genes and only a slight increase in six others. However, we also observed a higher-than-baseline indels frequencies in three genes—*C6ORF226,*

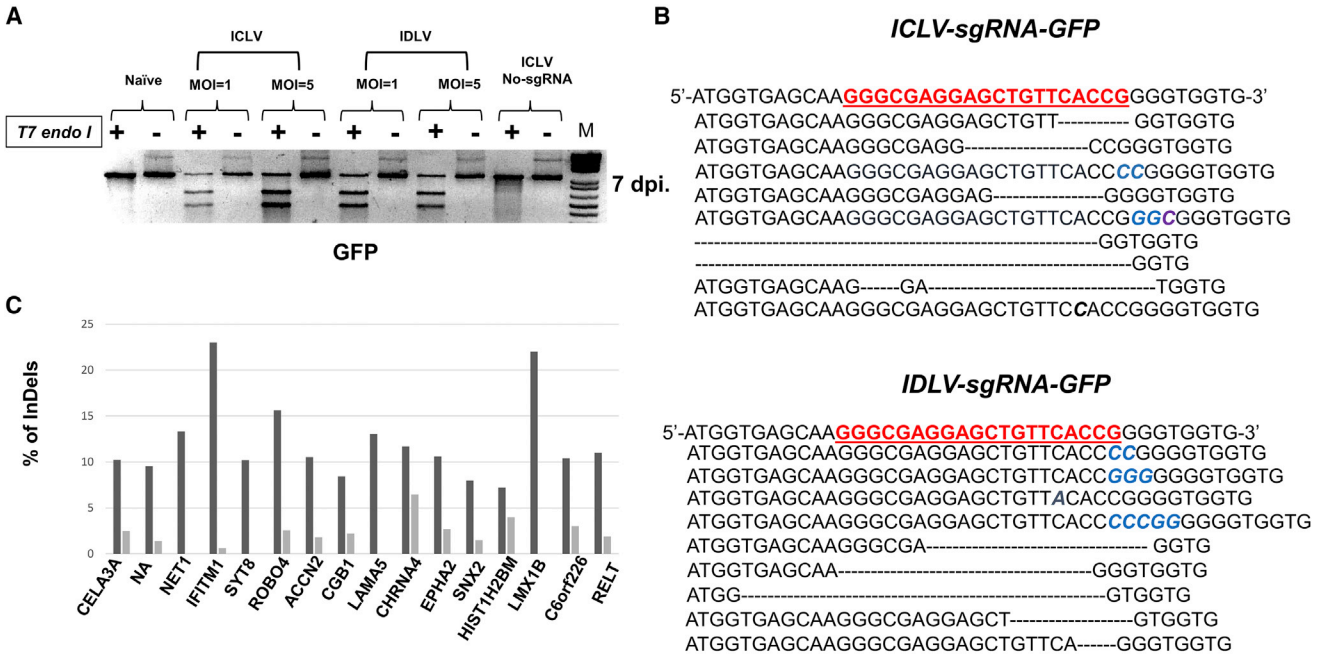

Figure 3. Comparison of Efficiency and Specificity of IDLV-CRISPR/Cas9 and ICLV-CRISPR/Cas9 Systems Using T7 Endonuclease I Assay, Sanger Sequencing, and WES

(A) On-target evaluation of DNA cleavages of CRISPR/Cas9 delivered by IDLV and ICLV. GFP-positive cells were transduced by IDLV-sgRNA1/Cas9 and ICLV-sgRNA1/Cas9 at varying MOIs and harvested at days 7 pt. The gDNA isolated from the transduced cells was amplified with GFP-specific primers and treated with T7 endo I (+) or left untreated (−). Naive, untransduced cells; M, molecular weight marker. (B) Sanger analysis of the ICLV- and IDLV-transduced samples. HEK293T cells were transduced by ICLV sgRNA-*gfp* or IDLV sgRNA-*gfp* at MOI = 1, and the rate of on-target mutations was determined at day 7 pt. The parental target sequence is highlighted in red. A representative sequencing analysis of nine clones (out of 50) is shown. The on-target insertions and deletions are underlined in blue and by dropped line, respectively. (C) Indels induced by ICLV-CRISPR/Cas9 (dark bars) and ICLV-CRISPR/Cas9 (light bars) were calculated as the ratio (in percentages) of reads with mutated sequences and total reads (see also Materials and Methods).

HIST1H2BM and *CHRNA4*—at the rates of 3%, 4%, and 6.47%, respectively (Figure 3C). Altogether, these results suggest that although transiently expressed IDLV-CRISPR/Cas9 is capable of inducing off-target mutations, it does so at significantly lower levels than ICLV-CRISPR/Cas9.

The Improved IDLV-sgRNA/Cas9 System Mediates Efficient and Specific Gene Editing in Dissociated Neurons

We sought to evaluate the efficacy of the novel IDLV-sgRNA/Cas9 platform by assessing the depletion GFP signal in dissociated post-mitotic neurons. To this end, we transduced the cells with GFP or mCherry-expressing lentiviral vectors, co-delivering IDLV-sgRNA1/Cas9 vector 1 day later. As shown in Figure S3, a robust depletion of the GFP was observed 10 days post-transduction with Sp1-IDLV vectors. Notably, significantly less depletion of the GFP signal was observed following delivery of CRISPR/Cas9 by the vector without Sp1 (Figure S3).

IDLV-Mediated sgRNA/Cas9 Gene Editing In Vivo

To verify the efficacy of the IDLV-sgRNA/Cas9 platform as an in vivo gene editing system, we targeted expression of a γ-amino-butyric acid A ($GABA_A$) receptor subunit α2 in the nucleus accumbens (NAc) of adult male Sprague-Dawley rats using an IDLV-α2/Cas9 vector. The NAc is a region in the ventral striatum implicated in processing of reward and relevant for clinical symptoms of drug abuse and major depressive disorders. The majority of neurons (95%) within the NAc synthesize GABA and express $GABA_A$ receptors that incorporate α1, α2, or α3 subunits localized to synaptic membranes.[52,53] Using western blotting, we detected α2-subunits in NAc tissue homogenates from control animals at levels similar to those previously observed.[54] At 35–47 days following microinjection of the IDLV α2/Cas9 vector, α2 protein declined to undetectable levels (Figure 4A). The identity of the α subunit confers distinct functional properties on the assembled $GABA_A$ receptor. Specifically, α2 and α3 subunit-containing $GABA_A$ receptors generate synaptic currents that last longer than those generated by α1 subunit-containing $GABA_A$ receptors.[53,55–57] We took advantage of this distinction to verify the efficiency of α2-knockout at the level of receptor function by measuring $GABA_A$ receptor-mediated miniature inhibitory postsynaptic currents (mIPSCs) in medium spiny neurons of the NAc. At 35–47 days following microinjection of the IDLV α2/Cas9, the duration of mIPSCs was characterized by broad cell-to-cell variability, contrasting sharply with the narrow distribution of mIPSC duration in cells from control animals (Figures 4B–4D). Distribution of mIPSC

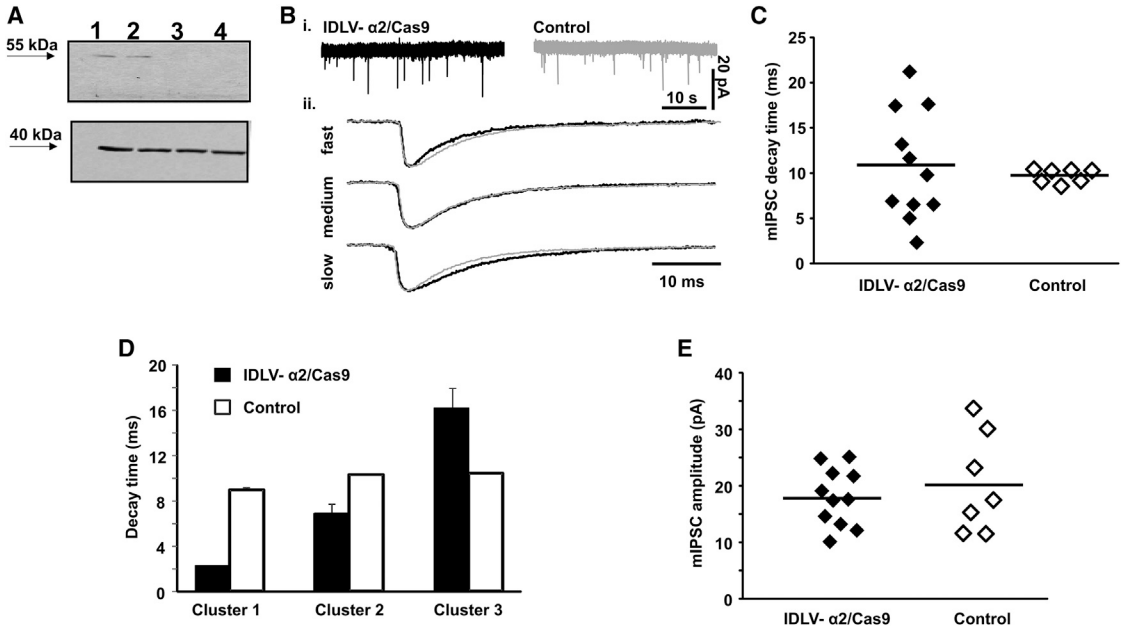

Figure 4. In Vivo Efficacy of IDLV-CRIPSR/Cas9 System

(A) Depletion of the $GABA_A$ receptor α2 subunit was confirmed by western blot analysis in two control (lanes 1 and 2) and two IDLV-α2/Cas9 injected (lanes 3 and 4) animals. Tubulin (DM1A) antibody was used as a loading control. (B) (i) Representative traces illustrating mIPSCs in NAc slices from control and IDLV-α2/Cas9-injected animals. Notice similar event frequency. (ii) mIPSC averages from three different neurons (black traces) illustrate variability of mIPSC duration in slices from IDLV-α2/Cas9 animals. Each trace is overlaid onto a mIPSCs average from a single control neuron (gray trace) for ease of comparison. (C) Distribution of mIPSC decay times from all recorded neurons. The horizontal black bars are centered at the mean values for each group. (D) K-means cluster analyses identify center values for slow, medium, and fast mIPSC groups of MSNs (n = 1, 5, and 5 IDLV-α2/Cas9 cells and n = 3, 2, and 2 control cells in clusters 1, 2, and 3, respectively). (E) Variability of mIPSC amplitudes is similar between cells in IDLV-α2/Cas9 and control groups. The horizontal black bars are centered at the mean values for each group.

amplitudes, an indicator of the number of post-synaptic receptors, was similar between IDLV α2/Cas9 and control groups (Figure 4E), and no differences in mIPSC frequency, a marker of presynaptic changes, were observed. These results indicate that IDLV α2/Cas9-induced knockout of $GABA_A$ receptor α2 subunits in the NAc was effective in altering the subunit composition of remaining $GABA_A$ receptors in the NAc, but did not change the number of post-synaptic receptors available for activation. Of greater relevance to this study, these findings highlight the utility of IDLV sgRNA/Cas9 platform for long-term reduction of gene function in non-dividing brain cells.

DISCUSSION

IDLVs present an attractive platform for viral-mediated gene transfer due to their numerous advantages over other delivery methods: (1) they are capable of efficiently transducing a broad range of cells and tissues, (2) they have large packaging capacity, (3) they demonstrate low cytotoxicity and immunogenicity, and (4) they retain very weak integration capacity and are transiently expressed from episomal genomes. These advantages make IDLVs a powerful tool in basic science and clinical research (reviewed in Kantor et al.,[6] and Wanisch and Yáñez-Muñoz[22]).[24,58]

Throughout this study, we sought to establish a single-molecule IDLV platform for efficient delivery of CRISPR/Cas9 components in vitro and in vivo. The advantages of lentiviral vectors used for CRISPR/Cas9 delivery are counterbalanced by the low titers associated with their production.[43] Therefore, we started by improving the titers of the all-in-one CRISPR/Cas9 system, to match those reported for the binary-CRISPR/Cas9 or naive vectors.[43] We demonstrated that the addition of an Sp1 binding site into all-in-one vector cassettes results in ~2.5-fold increase in the packaging efficiency of the vectors (Figure 1B) and ~7-fold increase in the overall functional production titers. The additional effect of Sp1 post-transfection (Figures 1B and 1C) suggests that this transcription factor may play a multifaceted role in the lentivirus life cycle. Such versatility is supported by earlier work from various groups highlighting Sp1 as a key transcriptional regulator of wild-type HIV-1.[44,46,47,59] Furthermore, Berkhout and colleagues[60] demonstrated that a vaccine-attenuated HIV strain was able to regain its replication fitness and virulence by duplicating Sp1 binding sites. It has also been shown that deletion of the Sp1 binding motif from viral LTRs and gag-intragenic regions results in dramatic loss of viral replication and infectivity.[45] Most of the available vector expression cassettes lack Sp1 binding sites and neither RNA Pol III promoters (e.g., U6 and H1), typically used to express sgRNA, nor viral core promoters (e.g., EFS-NC) expressing Cas9, harbor Sp1 binding sites. Thus, it would be interesting to determine whether addition of Sp1 to a relatively weak core promoter could substitute for the use of more powerful, but larger full-size counterparts. Based

on our results, we speculate that insertion of Sp1 binding sites could be adopted as a universal approach to enhance production, transcription, and infectivity of other viral systems used for delivering CRISPR/Cas9 cargoes. This approach could be especially valuable for smaller viruses (e.g., AAV), where limited packaging capacity precludes effective use. Furthermore, our findings become important in the context of IDLVs, since expression from episomal forms is generally lower than expression from the integrated genomes.[25,26] Indeed, we previously showed that IDLVs are organized into nucleosomal structures, enriched in histone modifications typical of silenced chromatin and thus subjected to layers of gene regulation involved in transcriptional silencing of cellular gene expression.[26]

We show that Sp1-CRISPR/Cas9 delivered by IDLVs can efficiently edit targeted sequences in the GFP-positive 293T cells. The rate and kinetics of GFP depletion were very similar to those observed for the integrase-wild-type vector. Furthermore, we found that short-term expression of CRISPR/Cas9 is sufficient to induce robust and permanent changes in the DNA. Indeed, we observed >80% of the cleavage activity within 7 days post-transduction and almost complete depletion of the GFP signal within 2 weeks. This observation is in line with previous work in which ribonucleoprotein complexes (Cas9 RNPs) were introduced into a variety of mammalian cells through liposome-mediated transfection and electroporation to achieve highly efficient genome cleavages within 2 days post transfection.[12] The study demonstrated rapid turnover and clearance of the transiently delivered sgRNA/Cas9.[12] Similarly, IDLVs induce only transient accumulation of episomal DNA in the nucleus, as they retain a very weak integration capacity compared to the integrating vectors. Nevertheless, IDLVs are capable of integrating into chromosomes due to illegitimate integrase-independent insertions at a low rate.[33] The rates of IDLV-CRISPR/Cas9 integration found in the current study were only slightly higher (0.8%), which suggests that CRISPR/Cas9 does not significantly enhance this rate. Our observations are in agreement with previous findings in which IDLVs have been used to detect and map off-target cleavages by CRISPR/Cas9 and TALEN systems.[61] In their study, Wang and colleagues[61] reported that co-delivery of IDLV and CRISPR/Cas9 (delivered as expression plasmids) induced a 2- to 3-fold increase in integration. Furthermore, the 1%–10% off-target indels formation reported in Wang et al.[61] is consistent with our observations of mild increase in the overall integration rate of IDLV-CRISPR/Cas9. Altogether, our results demonstrate that the episomal status of non-integrating vectors is not compromised by CRISPR/Cas9, and that the gene editing reported in Figure 2 arises from transient expression of the episomal vector.

Importantly, we report that episomal HIV-1 vectors are capable of attaining a strong and sustained CRISPR/Cas9 expression in dissociated post-mitotic neurons and in the rat brain (Figures 4 and S3). Using the improved IDLV-based system, we were able to efficiently and specifically knock down the GFP signal in cultured neurons and deplete the $GABA_A$ receptor α2 subunit protein in the nucleus accumbens shell. This depletion is associated with increased variability of observed mIPSC decay times in the recorded neurons. Duration of $GABA_A$ receptor-mediated mIPSCs depends on identity of the α subunit, as follows: α 3 > α 2 > α 1.[53,55–57] Therefore, the increased variability in mIPSC decay times that we observe may be due to compensatory upregulation of short-lasting synaptic currents mediated by α1-containing $GABA_A$ receptors and longer-lasting currents mediated by the α3-containing $GABA_A$ receptors. Importantly, a population of cells that continued to express α2-containing $GABA_A$ receptors may have contributed to these results, as our IDLV-α2/Cas9 construct did not incorporate a fluorescent tag that could enable positive identification of neurons transduced by the virus.

We demonstrate that IDLVs have improved specificity over ICLVs by measuring their off-target activities. Using WES analysis, we detected a total of 16 sequences in which delivery of CRISPR/Cas9 by integrating vectors has been associated with significantly higher rates of off-target indels than with the non-integrating vector (Figures 3C and S2). We demonstrated that following transduction with IDLV, minimal rates of indels (<3%) were observed in 13 genes (Figure 3C). Conversely, ICLVs showed significant increases in indels formation ranging from 3.4% to 24% (Figure 3C). The data are consistent with recent observations demonstrating that ICLV vectors delivering CRISPR/Cas9 induce high levels of indels.[11] Nevertheless, we report here that three genes, *C6ORF226*, *HIST1H2BM*, and *CHRNA4* showed a high level of indels (3%, 4%, and 6.5%, respectively) following delivery of CRISPR/Cas9 with IDLVs (Figure 3C). Interestingly, Hoban and colleagues[41] did not reveal off-target DNA cleavages in human $CD34^+$ cells using IDLV trapping-based strategy. However, the overall target specificity of the system was also low (∼20%). Indeed, efforts to modify CRISPR/Cas9 to enhance the specificity of the system without compromising on-target efficiency have not provided consistent results. For example, truncation of the 3′ end of sgRNA or addition of guanine nucleotides to the 5′ end of the sgRNA improves target specificity, decreasing undesired mutagenesis at some off-target sites by 5,000-fold.[13,62,63] However, these alterations also result in decreased on-target activity. Therefore, the system developed in this study constitutes a significant advance toward creation of both a specific and efficient CRISPR/Cas9 system. Additional developments based, for instance, on pairing IDLVs with safer endonucleases (e.g., Cas9-nickase, eSpCas9-, and SpCas9-HF), may further enhance this technology and will facilitate its therapeutic applications.[50,64,65] Our study represents the first evaluation of the efficiency of the IDLV-CRISPR/Cas9 system in post-mitotic neurons. Nevertheless, further and more comprehensive assessment of the long-term expressed Cas9 and sgRNA in non-dividing cells, in which episomal genomes are intrinsically stable, is required for better evaluation of the editing efficiency and specificity of our vector system.

MATERIALS AND METHODS

Plasmid Construction

Integrase-deficient packaging cassette was derived from psPAX2 (Addgene # 12260) and created as follows. The *int* region was amplified with the following primers: F- *5′-GAAATTTGTACAGAAATGG-3′*, and R- *5′-CTTCTAAATGTGTACAC-3′*. The R-primer harbored a

T-G mutation in the GAT-codon, which created a substitution of Asp (D) to Glu (E) - (D64E). The PCR product harboring the mutation was digested with *BsrGI* enzyme and was cloned into psPAX2 replacing the corresponding region. The *int-* packaging cassette was named pBK43. The plasmid sequence has been confirmed by sequencing analysis. To generate the short version of pLenti-CRISPR/Cas9-expressing cassette, the plasmid (Addgene # 52961) was digested with *BsmBI* and cloned with a pair of annealed and phosphorylated oligonucleotides, upper- *5′- CACCGGAGACGTGTACACGTCTCT-3′* and lower- *5′-AAAC AGAGACGTGTACACGTCTCC-3′*. The resulting plasmid, pBK109, harbored two *BsmBI* restriction enzyme sites separated by a short linker sequence. The *BsrGI* site created between *BsmBI* sites allowed for easy screening of sgRNA-positive clones. The plasmid was further modified to include a pair of Sp1 binding sites. To this end, the plasmid was digested with KpnI− and *PacI* and cloned with a pair of the annealed and the phosphorylated oligonucleotides, upper: *5′*-TA ATGGGCGGGACGTTAACGGGGCGGAACGGTAC-*3′* and lower: *5′*- CGTTCCGCCCCGTTAACGTCCCGCCCATTAAT-*3′*. The resulting plasmid was named pBK176. The following oligos were used to introduce sgRNAs targeting GFP into pBK109: (sgRNA1) upper: 5′-*CACCGGGGCGAGGAGCTGTTCACCG-3′*; lower: *5′*-AAACCGG TGAACAGCTCCTCGCCCC-*3′*; (sgRNA2) upper: *5′*-CACCGGGA GCGCACCATCTTCTTCA-*3′*; (sgRNA3) upper: *5′*- CACCGGGTG AACCGCATCGAGCTGA-*3′*; and lower: *5′*-AAACTGAGCTCGA TGCGGTTCACCC-*3′*. The resulting plasmids were digested with *NdeI* and cloned within the *NdeI-NdeI* fragment of pBK176 to include Sp1 sites. To introduce sgRNAs targeting α2 subunits of $GABA_A$ receptor, the following oligonucleotides were used: upper: 5′- CACC GTAATCGGCTTAGACCAGGAC-3′and lower: 5′-AAACGTCCT GGTCTAAGCCGATTAC-3′. To amplify the *eGFP* target region, the following primers were employed: F- *5′- CAAGTCTCCACCCC ATTGACG-3′* and R- *5′*-GAACTCCAGCAGGACCATGT-*3′*.

Vector Production

Lentiviral vectors were generated using the transient transfection protocol, as described previously.[33] Briefly, 15 μg vector plasmid, 10 μg psPAX2 packaging plasmid (Addgene #12260 generated in Dr. Didier Trono's lab, EPFL, Switzerland), 5 μg pMD2.G envelope plasmid (Addgene #12259, generated in Dr. Trono's lab), and 2.5 μg pRSV-Rev plasmid (Addgene #12253, generated in Dr. Trono's lab) were introduced into 293T cells by transfection. To generate IDLVs, a pBK43 (integrase-deficient) packaging cassette was used. Vector particles were collected from filtered conditioned medium at 72 hr post transfection. When necessary, the particles were purified using the sucrose-gradient method[33] and concentrated >100-fold by ultracentrifugation (2 hr at 22,000 rpm). Vector and viral stocks were aliquoted and stored at −80°C.

Titering Vector Preps

For integrating vectors expressing a fluorescent reporter (GFP), titers were determined using a p24 *gag*ELISA method and by counting GFP-positive cells, as described previously.[25] For non-integrating vectors and vectors carrying no reporter gene, the titers were determined using p^{24}*gag*ELISA equating 1 ng p^{24}*gag* to 1×10^4 viral particles. The multiplicity of infections (MOIs) was calculated as the ratio between the number of viral particles and number of cells. The p^{24}*gag* ELISA assay was carried out as per the instructions in the HIV-1 p^{24} Antigen Capture Assay Kit (NIH AIDS Vaccine Program). Briefly, high-binding 96-well plates (Costar) were coated with 100 μL monoclonal anti-p24 antibody obtained from the NIH AIDS Research and Reference Reagent Program (catalog # 3537), which was diluted 1:1,500 in PBS. Coated plates were incubated at 4°C overnight. Plates were blocked with 200 μL 1% bovine serum albumin (BSA) in PBS and washed three times with 200 μL 0.05% Tween 20 in cold PBS. Plates were incubated with 200 μL samples, inactivated by 1% Triton X-100 for 1 hr at 37°C. HIV-1 standards (catalog no. SP968F) were subjected to a 2-fold serial dilution and added to the plates at a starting concentration equal to 4 ng/mL. Samples were diluted in RPMI 1640 supplemented with 0.2% Tween 20 and 1% BSA applied to the plate and incubated at 4°C overnight. Plates were then washed six times and incubated at 37°C for 2 hr with 100 μL polyclonal rabbit anti-p^{24} antibody (catalog # SP451T), diluted 1:500 in RPMI 1640, 10% fetal bovine serum (FBS), 0.25% BSA, and 2% normal mouse serum (NMS; Equitech-Bio). Plates were washed as above and incubated at 37°C for 1 hr with goat anti-rabbit horseradish peroxidase IgG (Santa Cruz Biotechnology), diluted 1:10,000 in RPMI 1640 supplemented with 5% normal goat serum (NGS; Sigma), 2% NMS, 0.25% BSA, and 0.01% Tween 20. Plates were washed as above and incubated with TMB peroxidase substrate (KPL) at room temperature for 10 min. The reaction was stopped by adding 100 μL 1 N HCL. Plates were read by a microplate reader at 450 nm and analyzed in Excel. The experiments were performed in duplicate.

Flow Cytometry

HEK293T-eGFP cells were transduced with relevant vectors and examined for GFP fluorescence intensity. For fluorescence-activated cell sorting (FACS) analysis, cells were harvested using 0.05% trypsin-EDTA solution. The samples were precipitated by centrifugation at 2,000 rpm at 4°C, and the pellet was resuspended in 1 mL cold PBS. An equal volume of 4% formaldehyde solution was added to the samples for 10 min. Samples were washed once in PBS and harvested by centrifugation. The pellet was resuspended in 1 mL PBS. Samples were analyzed for GFP expression by the FACScan system (Becton Dickinson). Mean fluorescence intensity (MFI) and percentage of GFP-positive cells were determined. The experiments were performed in duplicate. We used naive (i.e., not transduced with GFP virus) cells to define a population of GFP-negative cells.

Western Blot Analysis

Nucleus accumbens shell was micro-dissected from 300-μM-thick coronal brain slices. The collected tissue was reverse-crosslinked to retrieve antigen epitopes and incubated with RIPA buffer (50 mM HEPES pH 7.6, 1 mM EDTA, 0.7% deoxycholate, 1% Nonidet P-40, and 0.5 M LiCl). Total protein amounts were determined by Lowry assay using BSA as a standard. Lysates were mixed with 1× Red Loading Buffer (catalog no. 7723; Cell Signaling Technology), supplemented with 100 mM DTT, and denatured by boiling for 10 min. Subsequently, SDS polyacrylamide gel electrophoresis was

performed followed by transfer to (NC/PVDF) membrane, which was later blocked by 5% non-fat dry milk for 60 min at room temperature with constant agitation. Anti-$GABA_A$ α2 Receptor antibody, #AGA-002, was acquired from Alomone Labs (Israel) and used at 1:250 dilutions. The reference control antibody was mouse α-Tubulin (DM1A) antibody (Cell Signaling Technologies) used at 1:1,000 dilution. The membrane was incubated with the antibody-containing solution for overnight at 4°C through gentle agitation. The membrane was then washed three times for 5 min each, after which, 0.05% Tween 20 in cold PBS (PBST) and the goat-anti-rabbit or goat-anti-mouse secondary antibodies were applied at dilution 1:10,000 for 1 hr at room temperature through gentle agitation. Blot detection was performed using an enhanced chemiluminescence (ECL) detection system (Pierce).

Real-Time PCR

To quantify rates of integration of IDLV and ICLV, we used the following qPCR-protocol. Genomic DNA was isolated from the transduced cells and digested with RNase A and DpnI overnight at 37°C. The following primers were used to amplify vector DNA: RRE-F- 5′-GCAACAGACATACAAAC-3′ and U6p-R- AAAACTGC AAACTACCCAAGAAA-3′. We used -beta-actin as a reference gene; Actin-F- 5′- AATCTGCCACCACACCTTC-3′ and Actin-R- 5′-GGG GTGTTGAAGGTCTCAAA-3′. iTaq Universal SYBR Green Supermix was used for the reactions (Bio-Rad). Real-time PCR was carried out using the iCycler iQ System (Bio-Rad), and the results were analyzed by iCycler software (Bio-Rad).

T7 Endonuclease I Assay

Genomic DNA was isolated and PCR-amplified as described above. The PCR-products were extracted and purified from the gel using QIAGEN gel extraction kit. There were 2 μL NEBuffer 2 and dH2O that were added for a total of 19 μL and subjected to a denaturation-renaturation cycle in a PCR cycler as follows: 5 min, 95°C; ramp down to 85°C at −2°C/s; ramp down to 25°C at −0.1°C/s; and hold at 4°C. Next, T7 endo I enzyme (NEB) was added (1 μL [10 U]) to the reaction mix, and the samples were incubated at 37°C for 1 hr. The reaction was stopped by adding 2 μL of 0.25 M EDTA and immediately loaded on a 1.2% agarose gel. The results were analyzed and quantified by E-Gel Imager System Software (Life Technologies).

Cell Culture

Human embryonic kidney (HEK293T) cells were obtained from ATCC (catalog number CRL-3216). Cells were grown in DMEM (Gibco), supplemented with 10% fetal bovine serum (Gibco), penicillin/streptomycin 1% (Thermo Fisher Scientific), 4.5 g/L D-glucose, 2mM L-glutamine, 1% MEM NEAA (Gibco), and 1 mM sodium pyruvate (Gibco). HEK293T-eGFP cells were generated by transduction of HEK293T cells with pLenti-GFP vector (vBK201a) at an MOI < 1 to ensure a transduction rate of <1 copy/cell; about 80% of the cells were found being GFP positive (data not shown). Mouse cortical neurons were seeded at 5×10^6 cells per 12-well plate. Neurons were cultured in Neurobasal Medium (Gibco) supplemented with 1× B27 (Gibco).

Fluorescent Microscopy

Mouse cortical neurons were seeded at 5×10^6 cells per 12-well plate as described above. The cells were transduced with pLenti-eGFP or pLenti-mCherry (1 × 106 viral particles)/well. At 24–30 hr post-transduction, cells were super-transduced with 2 × 106 viral particles/well of IDLV-no sgRNA/Cas9, IDLV-no Sp1/sgRNA-GFP1/Cas9, or IDLV-Sp1-sgRNA-GFP1/Cas9 vectors. Images were acquired 10 days post-transduction using Leica DM IRB Microscope/Imaging System (Leica Microsystems).

In Vivo Microinjections and Slice Electrophysiology

All animal protocols were approved by the University of South Carolina Institutional Animal Care and Use Committee. Adult male Sprague-Dawley rats (300–350 g) were anesthetized with intraperitoneal (i.p.) injections of a ketamine (80 mg/kg)/xylazine (12 mg/kg) mixture. IDLV-α2/Cas9 (2 μL) was injected bilaterally into the nucleus accumbens shell via a Neuros syringe (Hamilton) using the following stereotaxic coordinates (relative to bregma): 1.0 mm anterior, ± 1.0 mm lateral, and 7.0 mm ventral. At 35–47 days after virus microinjections, the rats were decapitated following isoflurane anesthesia. The brains were removed and coronal slices (300 μm) containing the nucleus accumbens shell were cut with a vibratome (VT1000S, Leica Microsystems) in an ice-cold artificial cerebrospinal fluid solution (ACSF), in which NaCl was replaced by an equi-osmolar concentration of sucrose. Control animals were treated similarly, but did not receive injection of the virus. ACSF consisted of 130 mM NaCl, 3 mM KCl, 1.25 mM NaH_2PO_4, 26 mM $NaHCO_3$, 10 mM glucose, 1 mM $MgCl_2$, and 2 mM $CaCl_2$ (pH7.2–7.4 when saturated with 95% O_2/5% CO_2). Slices were incubated in ACSF at 32°C–34°C for 45 min and kept at 22°C–25°C thereafter until transfer to the recording chamber. Slices were viewed using infrared differential interference contrast optics under an upright microscope (Eclipse FN1, Nikon Instruments) with a 40× water-immersion objective. The recording chamber was continuously perfused (1–2 mL/min) with oxygenated ACSF heated to 32 ± 1°C using an automatic temperature controller (Warner Instruments). DL-AP5 (50 μM) and DNQX (10 μM) were added to ACSF to block NMDA receptors and AMPA receptor, respectively. ACSF also contained TTX (0.5 μM) to block voltage-gated Na^+ channels and isolate action-potential independent mIPSCs. Recording pipettes were pulled from borosilicate glass capillaries (World Precision Instruments) to a resistance of 4–7 MΩ when filled with the intracellular solution. The intracellular solution contained (in mM): 100 $CsCH_3O_3S$, 50 CsCl, 3 KCl, 0.2 BAPTA, 10 HEPES, 1 $MgCl_2$, 2.5 phosphocreatine-2Na, 2 Mg-ATP, 0.25 GTP-Tris, and adjusted to pH 7.2–7.3 (pH 7.2–7.3 with CsOH and osmolarity 280–290 mOsm). Medium spiny neurons in the nucleus accumbens shell were identified by their morphology and the low resting membrane potential (−70 to −85 mV). mIPSC recordings were obtained in whole-cell voltage-clamp mode (Vh = −70 mV) using a MultiClamp700B amplifier (Molecular Devices). Currents were low-pass filtered at 2 kHz and digitized at 20 kHz using a Digidata 1440A acquisition board and pClamp 10 software (both from Molecular Devices). Access resistance (10–30 MΩ) was monitored

throughout the recordings by injection of 10 mV hyperpolarizing pulses, and data were discarded if access resistance changed by >25% over the course of data acquisition. All analyses of intracellular recordings were carried out with Clampfit 10 (Molecular Devices). The weighted time constant of decay was based on a double exponential fit to the decay phase of an average mIPSC trace computed from a minimum of 50 individual mIPSCs.

WES Analysis

293T cells were transduced with IDLV-*gfp*-sgRNA/Cas9 or/and ICLV-*gfp*-sgRNA/Cas9 at MOIs = 5 and harvested at day 21 pt. gDNA was isolated from the samples and hybridized to the probes of exome library (SeqCap EZ Library SR DNA-Seq; Roche). The library was pooled (4-plex), and exomes were enriched via NimbleGen protocol using SeqCap EZ Exome Enrichment Kit v3.0 (Roche). Each pool was sequenced in one Illumina HiSeq lane V4 (125 bp paired end) with on-target rates of ~65%. DNA-seq data underwent strict quality control with the TrimGalore package that removed all Illumina adaptor sequences or low quality base calls from the 3′ end of the reads. Reads were aligned to the hg19 version of the human genome with the BWA algorithm.[66] Alignment processing and variant calls were performed using GATK,[67,68] following the Broad Institute's Best Practices workflow.[69] Any indels present in at least one sample was reported along with the filtered read-depth supporting that particular indels across the samples.

SUPPLEMENTAL INFORMATION

Supplemental Information includes three figures and can be found with this article online at http://dx.doi.org/10.1016/j.omtm.2017.04.002.

AUTHOR CONTRIBUTIONS

B.K. and P.I.O. designed experiments, analyzed data, and wrote the manuscript; B.K., P.I.O., X.D., and B.O. executed experiments; B.K. supervised the study; and all of the authors discussed the results and assisted in the preparation of the manuscript.

CONFLICTS OF INTEREST

The University of South Carolina filed a provisional patent application related to this study.

ACKNOWLEDGMENTS

We thank Duke Center for genomic and computational biology and Sequencing and Genomic Technologies and Genomic Analysis and Bioinformatics Cores for performing and analyzing WES. We thank Udai Singh and the Flow Cytometry Core at the University of South Carolina for assistance. The all-in-one expression plasmid lenti-CRISPRv2 (Addgene plasmid #52961) was a kind gift from Feng Zhang (Broad Institute). We thank Sriram Vijayraghavan (Duke University) for his comments and help with manuscript preparation and submission. Support was provided by University of South Carolina-School of Medicine grant RDF18080-E202 (to B.K.) and National Institute on Drug Abuse (NIDA) grant K01 DA031747 (to P.I.O.).

REFERENCES

1. Horvath, P., and Barrangou, R. (2010). CRISPR/Cas, the immune system of bacteria and archaea. Science *327*, 167–170.
2. Marraffini, L.A., and Sontheimer, E.J. (2010). CRISPR interference: RNA-directed adaptive immunity in bacteria and archaea. Nat. Rev. Genet. *11*, 181–190.
3. Jinek, M., Chylinski, K., Fonfara, I., Hauer, M., Doudna, J.A., and Charpentier, E. (2012). A programmable dual-RNA-guided DNA endonuclease in adaptive bacterial immunity. Science *337*, 816–821.
4. Mali, P., Yang, L., Esvelt, K.M., Aach, J., Guell, M., DiCarlo, J.E., Norville, J.E., and Church, G.M. (2013). RNA-guided human genome engineering via Cas9. Science *339*, 823–826.
5. Cong, L., Ran, F.A., Cox, D., Lin, S., Barretto, R., Habib, N., Hsu, P.D., Wu, X., Jiang, W., Marraffini, L.A., and Zhang, F. (2013). Multiplex genome engineering using CRISPR/Cas systems. Science *339*, 819–823.
6. Kantor, B., Bailey, R.M., Wimberly, K., Kalburgi, S.N., and Gray, S.J. (2014). Methods for gene transfer to the central nervous system. Adv. Genet. *87*, 125–197.
7. Wang, W., Ye, C., Liu, J., Zhang, D., Kimata, J.T., and Zhou, P. (2014). CCR5 gene disruption via lentiviral vectors expressing Cas9 and single guided RNA renders cells resistant to HIV-1 infection. PLoS ONE *9*, e115987.
8. Kennedy, E.M., Bassit, L.C., Mueller, H., Kornepati, A.V., Bogerd, H.P., Nie, T., Chatterjee, P., Javanbakht, H., Schinazi, R.F., and Cullen, B.R. (2015). Suppression of hepatitis B virus DNA accumulation in chronically infected cells using a bacterial CRISPR/Cas RNA-guided DNA endonuclease. Virology *476*, 196–205.
9. Roehm, P.C., Shekarabi, M., Wollebo, H.S., Bellizzi, A., He, L., Salkind, J., and Khalili, K. (2016). Inhibition of HSV-1 replication by gene editing strategy. Sci. Rep. *6*, 23146.
10. Bellec, J., Bacchetta, M., Losa, D., Anegon, I., Chanson, M., and Nguyen, T.H. (2015). CFTR inactivation by lentiviral vector-mediated RNA interference and CRISPR-Cas9 genome editing in human airway epithelial cells. Curr. Gene Ther. *15*, 447–459.
11. Shalem, O., Sanjana, N.E., Hartenian, E., Shi, X., Scott, D.A., Mikkelsen, T.S., Heckl, D., Ebert, B.L., Root, D.E., Doench, J.G., and Zhang, F. (2014). Genome-scale CRISPR-Cas9 knockout screening in human cells. Science *343*, 84–87.
12. Kim, S., Kim, D., Cho, S.W., Kim, J., and Kim, J.S. (2014). Highly efficient RNA-guided genome editing in human cells via delivery of purified Cas9 ribonucleoproteins. Genome Res. *24*, 1012–1019.
13. Pattanayak, V., Lin, S., Guilinger, J.P., Ma, E., Doudna, J.A., and Liu, D.R. (2013). High-throughput profiling of off-target DNA cleavage reveals RNA-programmed Cas9 nuclease specificity. Nat. Biotechnol. *31*, 839–843.
14. Fu, B.X., Hansen, L.L., Artiles, K.L., Nonet, M.L., and Fire, A.Z. (2014). Landscape of target:guide homology effects on Cas9-mediated cleavage. Nucleic Acids Res. *42*, 13778–13787.
15. Hsu, P.D., Scott, D.A., Weinstein, J.A., Ran, F.A., Konermann, S., Agarwala, V., Li, Y., Fine, E.J., Wu, X., Shalem, O., et al. (2013). DNA targeting specificity of RNA-guided Cas9 nucleases. Nat. Biotechnol. *31*, 827–832.
16. Nelson, C.E., and Gersbach, C.A. (2016). Engineering delivery vehicles for genome editing. Annu. Rev. Chem. Biomol. Eng. *7*, 637–662.
17. Choi, J.G., Dang, Y., Abraham, S., Ma, H., Zhang, J., Guo, H., Cai, Y., Mikkelsen, J.G., Wu, H., Shankar, P., and Manjunath, N. (2016). Lentivirus pre-packed with Cas9 protein for safer gene editing. Gene Ther. *23*, 627–633.
18. Platt, R.J., Chen, S., Zhou, Y., Yim, M.J., Swiech, L., Kempton, H.R., Dahlman, J.E., Parnas, O., Eisenhaure, T.M., Jovanovic, M., et al. (2014). CRISPR-Cas9 knockin mice for genome editing and cancer modeling. Cell *159*, 440–455.
19. Truong, D.J., Kühner, K., Kühn, R., Werfel, S., Engelhardt, S., Wurst, W., and Ortiz, O. (2015). Development of an intein-mediated split-Cas9 system for gene therapy. Nucleic Acids Res. *43*, 6450–6458.
20. Ran, F.A., Cong, L., Yan, W.X., Scott, D.A., Gootenberg, J.S., Kriz, A.J., Zetsche, B., Shalem, O., Wu, X., Makarova, K.S., et al. (2015). In vivo genome editing using Staphylococcus aureus Cas9. Nature *520*, 186–191.
21. Kennedy, E.M., Kornepati, A.V., Mefferd, A.L., Marshall, J.B., Tsai, K., Bogerd, H.P., and Cullen, B.R. (2015). Optimization of a multiplex CRISPR/Cas system for use as an antiviral therapeutic. Methods *91*, 82–86.

22. Wanisch, K., and Yáñez-Muñoz, R.J. (2009). Integration-deficient lentiviral vectors: a slow coming of age. Mol. Ther. *17*, 1316–1332.

23. Hoban, M.D., Romero, Z., Cost, G.J., Mendel, M., Holmes, M., and Kohn, D.B. (2016). Delivery of genome editing reagents to hematopoietic stem/progenitor cells. Curr. Protoc. Stem Cell Biol. *36*, 5B.4.1–5B.4.10.

24. Negri, D.R., Michelini, Z., Bona, R., Blasi, M., Filati, P., Leone, P., Rossi, A., Franco, M., and Cara, A. (2011). Integrase-defective lentiviral-vector-based vaccine: a new vector for induction of T cell immunity. Expert Opin. Biol. Ther. *11*, 739–750.

25. Bayer, M., Kantor, B., Cockrell, A., Ma, H., Zeithaml, B., Li, X., McCown, T., and Kafri, T. (2008). A large U3 deletion causes increased in vivo expression from a non-integrating lentiviral vector. Mol. Ther. *16*, 1968–1976.

26. Kantor, B., Ma, H., Webster-Cyriaque, J., Monahan, P.E., and Kafri, T. (2009). Epigenetic activation of unintegrated HIV-1 genomes by gut-associated short chain fatty acids and its implications for HIV infection. Proc. Natl. Acad. Sci. USA *106*, 18786–18791.

27. Cornu, T.I., and Cathomen, T. (2007). Targeted genome modifications using integrase-deficient lentiviral vectors. Mol. Ther. *15*, 2107–2113.

28. Lombardo, A., Genovese, P., Beausejour, C.M., Colleoni, S., Lee, Y.L., Kim, K.A., Ando, D., Urnov, F.D., Galli, C., Gregory, P.D., et al. (2007). Gene editing in human stem cells using zinc finger nucleases and integrase-defective lentiviral vector delivery. Nat. Biotechnol. *25*, 1298–1306.

29. Michelini, Z., Negri, D.R., Baroncelli, S., Spada, M., Leone, P., Bona, R., Klotman, M.E., and Cara, A. (2009). Development and use of SIV-based Integrase defective lentiviral vector for immunization. Vaccine *27*, 4622–4629.

30. Joglekar, A.V., Hollis, R.P., Kuftinec, G., Senadheera, S., Chan, R., and Kohn, D.B. (2013). Integrase-defective lentiviral vectors as a delivery platform for targeted modification of adenosine deaminase locus. Mol. Ther. *21*, 1705–1717.

31. Coluccio, A., Miselli, F., Lombardo, A., Marconi, A., Malagoli Tagliazucchi, G., Gonçalves, M.A., Pincelli, C., Maruggi, G., Del Rio, M., Naldini, L., et al. (2013). Targeted gene addition in human epithelial stem cells by zinc-finger nuclease-mediated homologous recombination. Mol. Ther. *21*, 1695–1704.

32. Yi, G., Choi, J.G., Bharaj, P., Abraham, S., Dang, Y., Kafri, T., Alozie, O., Manjunath, M.N., and Shankar, P. (2014). CCR5 gene editing of resting CD4(+) T cells by transient ZFN expression from HIV envelope pseudotyped nonintegrating lentivirus confers HIV-1 resistance in humanized mice. Mol. Ther. Nucleic Acids *3*, e198.

33. Kantor, B., Bayer, M., Ma, H., Samulski, J., Li, C., McCown, T., and Kafri, T. (2011). Notable reduction in illegitimate integration mediated by a PPT-deleted, nonintegrating lentiviral vector. Mol. Ther. *19*, 547–556.

34. Apolonia, L., Waddington, S.N., Fernandes, C., Ward, N.J., Bouma, G., Blundell, M.P., Thrasher, A.J., Collins, M.K., and Philpott, N.J. (2007). Stable gene transfer to muscle using non-integrating lentiviral vectors. Mol. Ther. *15*, 1947–1954.

35. Philippe, S., Sarkis, C., Barkats, M., Mammeri, H., Ladroue, C., Petit, C., Mallet, J., and Serguera, C. (2006). Lentiviral vectors with a defective integrase allow efficient and sustained transgene expression in vitro and in vivo. Proc. Natl. Acad. Sci. USA *103*, 17684–17689.

36. Yáñez-Muñoz, R.J., Balaggan, K.S., MacNeil, A., Howe, S.J., Schmidt, M., Smith, A.J., Buch, P., MacLaren, R.E., Anderson, P.N., Barker, S.E., et al. (2006). Effective gene therapy with nonintegrating lentiviral vectors. Nat. Med. *12*, 348–353.

37. Suwanmanee, T., Hu, G., Gui, T., Bartholomae, C.C., Kutschera, I., von Kalle, C., Schmidt, M., Monahan, P.E., and Kafri, T. (2014). Integration-deficient lentiviral vectors expressing codon-optimized R338L human FIX restore normal hemostasis in Hemophilia B mice. Mol. Ther. *22*, 567–574.

38. Negri, D.R., Michelini, Z., Baroncelli, S., Spada, M., Vendetti, S., Buffa, V., Bona, R., Leone, P., Klotman, M.E., and Cara, A. (2007). Successful immunization with a single injection of non-integrating lentiviral vector. Mol. Ther. *15*, 1716–1723.

39. Rossi, A., Michelini, Z., Leone, P., Borghi, M., Blasi, M., Bona, R., Spada, M., Grasso, F., Gugliotta, A., Klotman, M.E., et al. (2014). Optimization of mucosal responses after intramuscular immunization with integrase defective lentiviral vector. PLoS ONE *9*, e107377.

40. Karwacz, K., Mukherjee, S., Apolonia, L., Blundell, M.P., Bouma, G., Escors, D., Collins, M.K., and Thrasher, A.J. (2009). Nonintegrating lentivector vaccines stimulate prolonged T-cell and antibody responses and are effective in tumor therapy. J. Virol. *83*, 3094–3103.

41. Hoban, M.D., Lumaquin, D., Kuo, C.Y., Romero, Z., Long, J., Ho, M., Young, C.S., Mojadidi, M., Fitz-Gibbon, S., Cooper, A.R., et al. (2016). CRISPR/Cas9-mediated correction of the sickle mutation in human CD34+ cells. Mol. Ther. *24*, 1561–1569.

42. Maeder, M.L., and Gersbach, C.A. (2016). Genome-editing technologies for gene and cell therapy. Mol. Ther. *24*, 430–446.

43. Sanjana, N.E., Shalem, O., and Zhang, F. (2014). Improved vectors and genome-wide libraries for CRISPR screening. Nat. Methods *11*, 783–784.

44. Van Lint, C., Ghysdael, J., Paras, P., Jr., Burny, A., and Verdin, E. (1994). A transcriptional regulatory element is associated with a nuclease-hypersensitive site in the pol gene of human immunodeficiency virus type 1. J. Virol. *68*, 2632–2648.

45. Van Lint, C., Amella, C.A., Emiliani, S., John, M., Jie, T., and Verdin, E. (1997). Transcription factor binding sites downstream of the human immunodeficiency virus type 1 transcription start site are important for virus infectivity. J. Virol. *71*, 6113–6127.

46. Goffin, V., Demonté, D., Vanhulle, C., de Walque, S., de Launoit, Y., Burny, A., Collette, Y., and Van Lint, C. (2005). Transcription factor binding sites in the pol gene intragenic regulatory region of HIV-1 are important for virus infectivity. Nucleic Acids Res. *33*, 4285–4310.

47. Kim, Y.S., Kim, J.M., Jung, D.L., Kang, J.E., Lee, S., Kim, J.S., Seol, W., Shin, H.C., Kwon, H.S., Van Lint, C., et al. (2005). Artificial zinc finger fusions targeting Sp1-binding sites and the trans-activator-responsive element potently repress transcription and replication of HIV-1. J. Biol. Chem. *280*, 21545–21552.

48. Crosetto, N., Mitra, A., Silva, M.J., Bienko, M., Dojer, N., Wang, Q., Karaca, E., Chiarle, R., Skrzypczak, M., Ginalski, K., et al. (2013). Nucleotide-resolution DNA double-strand break mapping by next-generation sequencing. Nat. Methods *10*, 361–365.

49. Bonner, W.M., Redon, C.E., Dickey, J.S., Nakamura, A.J., Sedelnikova, O.A., Solier, S., and Pommier, Y. (2008). GammaH2AX and cancer. Nat. Rev. Cancer *8*, 957–967.

50. Ran, F.A., Hsu, P.D., Lin, C.Y., Gootenberg, J.S., Konermann, S., Trevino, A.E., Scott, D.A., Inoue, A., Matoba, S., Zhang, Y., and Zhang, F. (2013). Double nicking by RNA-guided CRISPR Cas9 for enhanced genome editing specificity. Cell *154*, 1380–1389.

51. Fu, Y., Foden, J.A., Khayter, C., Maeder, M.L., Reyon, D., Joung, J.K., and Sander, J.D. (2013). High-frequency off-target mutagenesis induced by CRISPR-Cas nucleases in human cells. Nat. Biotechnol. *31*, 822–826.

52. Wisden, W., Laurie, D.J., Monyer, H., and Seeburg, P.H. (1992). The distribution of 13 GABAA receptor subunit mRNAs in the rat brain. I. Telencephalon, diencephalon, mesencephalon. J. Neurosci. *12*, 1040–1062.

53. Ortinski, P.I., Lu, C., Takagaki, K., Fu, Z., and Vicini, S. (2004). Expression of distinct alpha subunits of GABAA receptor regulates inhibitory synaptic strength. J. Neurophysiol. *92*, 1718–1727.

54. Chen, Q., Lee, T.H., Wetsel, W.C., Sun, Q.A., Liu, Y., Davidson, C., Xiong, X., Ellinwood, E.H., and Zhang, X. (2007). Reversal of cocaine sensitization-induced behavioral sensitization normalizes GAD67 and GABAA receptor alpha2 subunit expression, and PKC zeta activity. Biochem. Biophys. Res. Commun. *356*, 733–738.

55. Gingrich, K.J., Roberts, W.A., and Kass, R.S. (1995). Dependence of the GABAA receptor gating kinetics on the alpha-subunit isoform: implications for structure-function relations and synaptic transmission. J. Physiol. *489*, 529–543.

56. Lavoie, A.M., Tingey, J.J., Harrison, N.L., Pritchett, D.B., and Twyman, R.E. (1997). Activation and deactivation rates of recombinant GABA(A) receptor channels are dependent on alpha-subunit isoform. Biophys. J. *73*, 2518–2526.

57. Barberis, A., Mozrzymas, J.W., Ortinski, P.I., and Vicini, S. (2007). Desensitization and binding properties determine distinct alpha1beta2gamma2 and alpha3beta2gamma2 GABA(A) receptor-channel kinetic behavior. Eur. J. Neurosci. *25*, 2726–2740.

58. Kantor, B., McCown, T., Leone, P., and Gray, S.J. (2014). Clinical applications involving CNS gene transfer. Adv. Genet. *87*, 71–124.

59. Gómez-Gonzalo, M., Carretero, M., Rullas, J., Lara-Pezzi, E., Aramburu, J., Berkhout, B., Alcamí, J., and López-Cabrera, M. (2001). The hepatitis B virus X protein induces HIV-1 replication and transcription in synergy with T-cell activation signals: functional roles of NF-kappaB/NF-AT and SP1-binding sites in the HIV-1 long terminal repeat promoter. J. Biol. Chem. *276*, 35435–35443.

60. Berkhout, B., Verhoef, K., van Wamel, J.L., and Back, N.K. (1999). Genetic instability of live, attenuated human immunodeficiency virus type 1 vaccine strains. J. Virol. *73*, 1138–1145.

61. Wang, X., Wang, Y., Wu, X., Wang, J., Wang, Y., Qiu, Z., Chang, T., Huang, H., Lin, R.J., and Yee, J.K. (2015). Unbiased detection of off-target cleavage by CRISPR-Cas9 and TALENs using integrase-defective lentiviral vectors. Nat. Biotechnol. *33*, 175–178.

62. Cho, S.W., Kim, S., Kim, Y., Kweon, J., Kim, H.S., Bae, S., and Kim, J.S. (2014). Analysis of off-target effects of CRISPR/Cas-derived RNA-guided endonucleases and nickases. Genome Res. *24*, 132–141.

63. Fu, Y., Sander, J.D., Reyon, D., Cascio, V.M., and Joung, J.K. (2014). Improving CRISPR-Cas nuclease specificity using truncated guide RNAs. Nat. Biotechnol. *32*, 279–284.

64. Slaymaker, I.M., Gao, L., Zetsche, B., Scott, D.A., Yan, W.X., and Zhang, F. (2016). Rationally engineered Cas9 nucleases with improved specificity. Science *351*, 84–88.

65. Kleinstiver, B.P., Pattanayak, V., Prew, M.S., Tsai, S.Q., Nguyen, N.T., Zheng, Z., and Joung, J.K. (2016). High-fidelity CRISPR-Cas9 nucleases with no detectable genome-wide off-target effects. Nature *529*, 490–495.

66. Li, H., and Durbin, R. (2009). Fast and accurate short read alignment with Burrows-Wheeler transform. Bioinformatics *25*, 1754–1760.

67. McKenna, A., Hanna, M., Banks, E., Sivachenko, A., Cibulskis, K., Kernytsky, A., Garimella, K., Altshuler, D., Gabriel, S., Daly, M., and DePristo, M.A. (2010). The genome analysis toolkit: a MapReduce framework for analyzing next-generation DNA sequencing data. Genome Res. *20*, 1297–1303.

68. DePristo, M.A., Banks, E., Poplin, R., Garimella, K.V., Maguire, J.R., Hartl, C., Philippakis, A.A., del Angel, G., Rivas, M.A., Hanna, M., et al. (2011). A framework for variation discovery and genotyping using next-generation DNA sequencing data. Nat. Genet. *43*, 491–498.

69. Van der Auwera, G.A., Carneiro, M.O., Hartl, C., Poplin, R., Del Angel, G., Levy-Moonshine, A., Jordan, T., Shakir, K., Roazen, D., Thibault, J., et al. (2013). From FastQ data to high confidence variant calls: the Genome Analysis Toolkit best practices pipeline. Curr. Protoc. Bioinformatics *43*, 11.10.11–11.10.33.